Temperature-Dependent Rate and Equilibrium Constants for Br • (aq) + Br − (aq) ↔ Br 2 −• (aq)

ARTICLE *in* THE JOURNAL OF PHYSICAL CHEMISTRY A · NOVEMBER 2002

Impact Factor: 2.69 · DOI: 10.1021/jp0255536

Temperature-Dependent Rate and Equilibrium Constants for $Br^{\bullet}(aq) + Br^{-}(aq) \leftrightarrow Br_2^{-\bullet}(aq)$

Yong Liu, Andre S. Pimentel,[†] Yasuko Antoku,[‡] Brent J. Giles,[§] and John R. Barker*,[||]

Department of Atmospheric, Oceanic, and Space Sciences, University of Michigan, Ann Arbor, Michigan 48109-2143

Received: January 28, 2002; In Final Form: July 29, 2002

Aqueous bromine atoms were produced by laser flash photolysis of 1,2-dibromoethane at 248 nm in solutions containing bromide ions. Forward and reverse rate constants of the title reaction were determined as functions of temperature. An analysis of potential sources of systematic errors shows that the measured forward and reverse rate constants have relative uncertainties ($\pm\sigma_k/k$) of ~10 and ~25%, respectively, over the temperature range from 10.5 to 50 °C. The Arrhenius parameters are ($k_f \pm 10\%$) = 5.1×10^{12} exp ($-1812/T$) M^{-1} s^{-1} and ($k_r \pm 25\%$) = 2.5×10^{10}exp ($-4068/T$) s^{-1}. The equilibrium constant is found from the ratio of k_f/k_r: ($K_{eq} \pm 30\%$) = 2.0×10^2 exp ($2256/T$) M^{-1} or (3.9 ± 1.2) $\times 10^5$ M^{-1} at 298 K. The reaction entropy and enthalpy are $\Delta S_R° = 44 \pm 6$ J mol^{-1} K^{-1} and $\Delta H_R° = -19 \pm 2$ kJ mol^{-1}, respectively. The corresponding reaction reduction potential is $\Delta E° = 0.33 \pm 0.01$ V, in very good agreement with that calculated from half-cell potentials. In addition, preliminary rate constants for $Br_2^{-\bullet} + Br_2^{-\bullet} \rightarrow Br_3^- + Br^-$ and the hydrogen abstraction reaction ($Br^{\bullet} + BrCH_2CH_2Br \rightarrow {}^{\bullet}CBrH-CH_2-Br + H^+ + Br^-$) are reported.

1. Introduction

There is considerable interest in the chemical conversion of the halide salts found in atmospheric sea salt aerosols to photochemically labile halogen species that are released into the gas phase. For example, bromine- and chlorine-containing species have been implicated in the episodes of sudden and near-complete depletion of ozone observed in the marine boundary layer in polar regions shortly after the Spring equinox.[1−3] The halogens found in the compounds are thought to originate from sea salt aerosols: several oxidation−reduction chemical mechanisms have been proposed to explain "halogen activation", in which dissolved halides are oxidized to produce photochemically labile halogen-containing compounds that can be photolyzed, hence initiating a gas phase chain reaction destroying ozone.[4−10]

It is also possible that aqueous free radical reactions participate in halogen activation. When, for example, hydroxyl radicals are produced by photolysis of hydrogen peroxide in aqueous solutions containing dissolved halides, the following reactions ensue in the solution (X = Cl, Br):[11−14]

$$^{\bullet}OH + X^- \leftrightarrow XOH^{-\bullet} \quad (1)$$

$$XOH^{-\bullet} + H^+ \leftrightarrow X^{\bullet} + H_2O \quad (2)$$

$$X^{\bullet} + X^- \leftrightarrow X_2^{-\bullet} \quad (3)$$

Dihalide radical anions ($X_2^{-\bullet}$) have been studied for many years both in biological and in simple inorganic systems.[15−17] They are known to react in various ways to produce molecular halogens and other photochemically labile halogen species. Reactions 4a,b, for example, are well-known[12]

$$X_2^{-\bullet} + X_2^{-\bullet} \rightarrow X_3^- + X^- \quad (4a)$$

$$X_3^- \rightarrow X_2 + X^- \quad (4b)$$

The molecular halogen may react further in solution, or it may escape into the gas phase, where it can be photolyzed.

In seawater and in fresh sea salt aerosols, the acidity is relatively low (pH ≈ 8), but in aged sea salt aerosols, the acidity can be much higher due to the release of H^+ produced in the oxidation of sulfur compounds.[18] Although the chloride concentration in seawater is more than 600 times that of bromide, reaction 2 for X = Cl is much slower than for X = Br, and when the pH is high, the bromine reactions dominate.[19] At lower pH, the chlorine reaction may become dominant. Thus, both chlorine and bromine species are important but under different conditions. In both cases, the equilibrium defined by reaction 3 is important because it regulates the relative concentrations of solvated $X^{\bullet}$ atoms, which are highly reactive, and $X_2^{-\bullet}$ radical anions, which are less reactive.[12] Because the equilibrium in reaction 3 is so important, the equilibrium constant for X = Cl at room temperature has been the subject of several investigations,[11,20−22] including one from this laboratory.[13] Three of these investigations[11,13,22] agree that $K_3 \approx 1.4 \times 10^5$ M^{-1} for X = Cl (in this paper, equilibrium constants are denoted with upper case *K*, while rate constants are denoted with lower case *k*). Despite its importance in free radical systems that contain bromide, agreement has not been reached for the X = Br case. The reported values[23−29] of the equilibrium constant for reaction 3 with X = Br range over 3 orders of magnitude, and the temperature dependence has only been reported once,[29] prior to the present work.

In the following, we describe measurements of the forward and reverse rate constants of reaction 3 for X = Br as functions of temperature and pH. The temperature-dependent equilibrium constant is obtained as the ratio $K_{eq}(T) = k_f(T)/k_r(T)$, experimental errors are assessed, and all quantities are compared with values from the literature.

* To whom correspondence should be addressed. E-mail: jrbarker@umich.edu.

[†] Present address: Laboratory for Extraterrestrial Physics (Code 690), NASA/Goddard Space Flight Center, Greenbelt, MD 20771.

[‡] Department of Chemistry, Fairmont State College, Fairmont, WV 26554.

[§] Present address: Department of Chemistry, Colorado College, Colorado Springs, CO 80904.

[||] Also a member of the Department of Chemistry.

10.1021/jp0255536 CCC: $22.00
Published on Web 10/23/2002

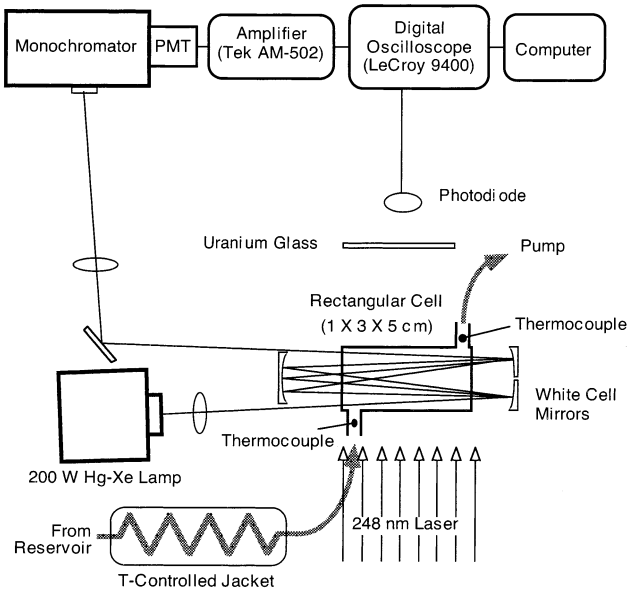

Figure 1. Experimental apparatus. For clarity, not all components are shown.

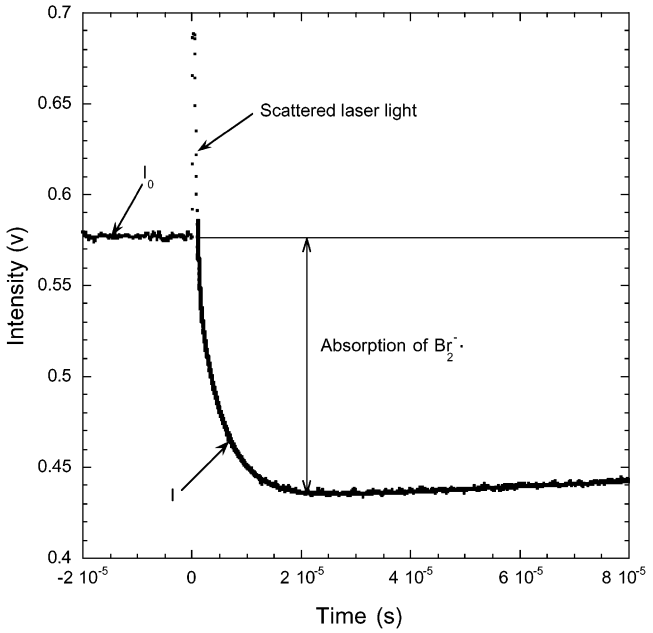

Figure 2. Typical time-dependent $Br_2^{-\bullet}$ absorption data (points) and fitted curve (solid line) for $[Br^-] = 3 \times 10^{-5}$ M. The absorbance corresponds to $[Br^\bullet]_0 \approx 2 \times 10^{-7}$ M.

2. Experimental Section

The experimental apparatus is shown schematically in Figure 1. It consisted of a combination of excimer laser flash photolysis and time-resolved detection of transient species by multipass absorbance. The photolysis light source was pulsed 248 nm radiation from a KrF excimer laser (Lumonics HyperEx-400). The laser was typically operated at 0.2 Hz with output energy of up to ~40 mJ per pulse. The laser beam was passed through a rectangular mask (2.0 cm × 4.7 cm) and illuminated the reaction cell. The rectangular reaction cell had an internal volume of ~15 cm^3 (1 cm × 3 cm × 5 cm) and was fabricated from polished fused silica (Suprasil) windows; the exterior surfaces had an antireflection coating. Reaction mixtures were prepared in volumetric flasks and pumped through the cell by a peristaltic pump (Masterflex model 7553-70) located downstream from the cell. The solution was not recirculated. At the typical volume flow rate of 2.5 cm^3/s, cavitation did not occur. The solutions came into contact only with Teflon and borosilicate glass upstream of the cell.

Prior to flowing into the cell, the solution passed through a glass helical condenser with a temperature-controlled water-jacket. Temperature control of the water-jacket was achieved by using a recirculating constant temperature bath (FTS Systems). Temperature was measured by two calibrated copper−constantan thermocouples in glass thermocouple wells at the cell entrance and exit. The temperatures quoted in the results were determined by averaging readings from the two thermocouples. Typically, the two temperatures differed by less than 0.5 °C, except at the extreme ends of the experimental temperature range, where the differences were still less than 1.5 °C.

The analytical light source was a 200 W Hg−Xe arc lamp (Oriel model 6291). Light from the lamp was passed through a liquid water filter to remove infrared radiation and then through a 400 nm cutoff filter (Oriel Filters 51265) to eliminate most of the UV fraction. A White cell with two end mirrors of 15 cm radius of curvature was used to increase the optical path length and therefore the signal-to-noise ratio; 12 passes (~60 cm path length) were used in most of the experiments. After it was passed through the cell, the analytical light was directed to the monochromator (Jarrell−Ash model 82-497) by first surface mirrors and focused on the monochromator entrance with a plano-convex Suprasil lens of focal length 200 ± 2 mm (Newport, SPX028). The monochromator was set to monitor the strong lamp emission near 365 nm; the intensity was measured using a photomultiplier tube (Hamamatsu 1P28) equipped with a resistor chain and socket designed for high-speed response (Hamamatsu E717-05). The photomultiplier anode current was maintained at less than ~4 μA to ensure response linearity. The anode current signal was passed through a 1.2 K Ω load resistor, and the resulting voltage signal was first amplified (Tektronix AM502) and then captured and averaged with a digital oscilloscope (LeCroy 9400). The instrument response time constant was ~0.3 or ~0.5 μs, depending on the electronic filter selected with the AM502 preamplifier. Signals were averaged for 100−150 laser shots by the oscilloscope and stored on a Macintosh computer (Apple Computer, Inc.) for further analysis. The oscilloscope was triggered by a silicon photodiode (Thorlabs Inc. DET2-S1) that viewed the laser output. In some experiments, wire screens were used to attenuate the laser intensity. By using the pretrigger feature of the oscilloscope, the transmitted 365 nm intensity I_0 prior to the laser pulse was recorded, as well as the time-dependent intensity $I(t)$ following the pulse, as shown in Figure 2.

All solutions were freshly prepared just before the experiments. The water was purified by a Millipore Milli-Q system, and the resistivity was >16 M Ω cm. The chemicals used in this study had the following grade and stated minimum purities: NaBr (Aldrich), >99%, certified; $HClO_4$ (Fisher), 70%, reagent ACS; 1,2-dibromoethane (DBE) (Aldrich), 99%, ACS reagent. A key requirement for these experiments was that the bromide ion concentrations must be known accurately. Because DBE contains 1% impurities and may undergo hydrolysis in aqueous solution to produce dissolved bromide ion, the DBE was washed immediately before use in order to minimize potential contamination. About 3−5 mL of DBE, which is only slightly soluble in water, was shaken vigorously with water in a volumetric flask for 1 min. After the solution was allowed to stand for 5 min, the water was decanted to remove water soluble impurities, leaving the washed DBE in the flask. More water was then added to the washed DBE, and the mixture was stirred for 10 min to produce a "saturated" solution. Experiments

showed that the solution appeared to approach saturation after about 10 min of stirring, as judged by photolytic yields of $Br_2^{-\bullet}$. Stirring for extended times (e.g., ~1 h) seemed to result in the generation of bromide impurities, perhaps due to hydrolysis of DBE. In most experiments, the saturated DBE solution was diluted with water to 1/10 of its original concentration, giving [DBE] $\approx 2.1 \times 10^{-3}$ M. Bromide ion concentrations were adjusted as desired in the range of $(0.5-5) \times 10^{-5}$ M by adding weighed quantities of NaBr. The acidity of the solutions was adjusted by adding perchloric acid ($HClO_4$).

The solubility of DBE was verified as a function of temperature by adding weighed quantities of DBE dropwise to a quantity of purified water. The resulting solubility at 20 °C (~0.40 g/100 g H_2O) was in good agreement with a reported value,[30] and the derivative of DBE solubility with respect to temperature was found to be $\sim 2.6 \times 10^{-3}$ K^{-1}.

3. Results

3.1. Chemical Mechanism and Data Analysis. Bromine atoms were generated by 248 nm laser flash photolysis of dissolved DBE:[31,32]

$$BrCH_2CH_2Br + h\nu \rightarrow C_2H_4 + 2\,Br^{\bullet} \qquad (5)$$

When $[Br^-]$ is present, an immediate increase in the absorbance at 365 nm is observed following the laser pulse, followed by a slow decay back to the initial intensity, as shown in Figure 2. The absorption is due to $Br_2^{-\bullet}$, which has an absorption coefficient (base 10) $\alpha = 9600$ M^{-1} cm^{-1} at 365 nm.[33] The reaction mechanism is as follows:

$$Br^{\bullet} + Br^- \rightarrow Br_2^{-\bullet} \qquad (6)$$

$$Br_2^{-\bullet} \rightarrow Br^{\bullet} + Br^- \qquad (-6)$$

$$Br_2^{-\bullet} + Br_2^{-\bullet} \rightarrow Br_3\text{-} + Br^- \qquad (7a)$$

$$Br_3^- \leftrightarrow Br_2 + Br^- \qquad (7b)$$

$$DBE + Br^{\bullet} \rightarrow {}^{\bullet}CBrH{-}CH_2{-}Br + H^+ + Br^- \qquad (8)$$

$$DBE + Br_2^{-\bullet} \rightarrow {}^{\bullet}CBrH{-}CH_2{-}Br + H^+ + 2Br^- \qquad (9)$$

The time-dependent transmitted pulse light intensity $I(t)$ depends on the absorbance $A(t)$ according to the Beer−Lambert equation:

$$(I(t)/I_0) = 10^{-A(t)} = 10^{-\alpha s[Br_2^{-\bullet}]} \qquad (10)$$

where I_0 is the initial intensity, s is the optical path length (~60 cm), and α is the optical absorption coefficient; the square brackets denote concentrations.

To analyze the time-dependent transmitted intensity, the chemical mechanism is used to derive an approximate analytical expression for the time-dependent $[Br_2^{-\bullet}]$. The reaction mechanism is comprised of reactions 6, −6, 7, 8, and 9. The resulting coupled differential equations are

$$(d[Br_2^{-\bullet}]/dt) = k_6[Br^{\bullet}][Br^-] - k_{-6}[Br_2^{-\bullet}] - 2k_7[Br_2^{-\bullet}]^2 - k_9[DBE][Br_2^{-\bullet}] \qquad (11a)$$

$$(d[Br^{\bullet}]/dt) = k_{-6}[Br_2^{-\bullet}] - k_6[Br^{\bullet}][Br^-] - k_8[DBE][Br^{\bullet}] \qquad (11b)$$

A convenient analytical solution to these equations can be found if the term that contains $[Br_2^{-\bullet}]^2$ is neglected or replaced by an approximate expression. The magnitude of the second-order term is small under the conditions of the experiments. In all of the experiments (see Figure 2, for example), the ultimate decay of absorption is much slower than the initial rise; thus, it would be possible to neglect the second-order term at some sacrifice of accuracy. A better approach is to use an approximation that accounts to some extent for the decay of $[Br_2^{-\bullet}]$, such as the following first-order approximation:

$$2k_7[Br_2^{-\bullet}]^2 \approx 2k_7[Br_2^{-\bullet}]_{avg}[Br_2^{-\bullet}] = \gamma[Br_2^{-\bullet}] \qquad (12)$$

where $[Br_2^{-\bullet}]_{avg}$ is an average concentration and γ is therefore a constant.

This approximation is accurate when $[Br_2^{-\bullet}]$ varies only slightly, but it is less accurate when $[Br_2^{-\bullet}]$ is varying rapidly. Even in the latter case, the second-order term is small as compared to the other terms in eq 11a and the approximation is acceptable for determining rate constants k_6 and k_{-6} (numerical tests are described below). With this approximation, the coupled equations can be solved (e.g., by using Laplace transforms) to obtain $[Br_2^{-\bullet}]$:

$$[Br_2^{-\bullet}] = (k_6[Br^-][Br^{\bullet}]_0)(e^{r_1 t} - e^{r_2 t})/(r_1 - r_2) \qquad (13a)$$

$$A = \{k_a^{I} + \gamma\} \qquad (13b)$$

$$B = \{k_6[Br^-](\gamma + k_8[DBE]) + k_9[DBE](k_{-6} + \gamma + k_8[DBE])\} \qquad (13c)$$

$$k_a^{I} = k_{-6} + k_6[Br^-] + (k_8 + k_9)[DBE] \qquad (13d)$$

where r_1 and r_2 are roots of the quadratic equation $p^2 + Ap + B = 0$, p is the Laplace transform variable, $[Br^{\bullet}]_0$ is the concentration of bromine atoms generated by the photolysis of DBE, and k_a^{I} is a pseudo-first-order rate constant. For the present experimental conditions, rate constants k_6, k_{-6}, γ, k_8, and k_9 are of the order of 10^{10} M^{-1} s^{-1}, 10^4 s^{-1}, 10^3 s^{-1}, 10^6 M^{-1} s^{-1}, and $\ll 10^6$ M^{-1} s^{-1}, respectively (k_8 and k_9 are discussed below). Therefore, the following inequality holds

$$A^2 \gg 4B \qquad (14)$$

and the roots of the quadratic equation can be approximated as $r_1 \approx (k_a^{I} + \gamma)$ and $r_2 \approx \gamma$. Thus, $[Br_2^{-\bullet}]$ as a function of time is given as

$$[Br_2^{-\bullet}] = k_6[Br^-][Br^{\bullet}]_0 \frac{e^{-(k_a^{I}+\gamma)t} - e^{-\gamma t}}{k_a^{I}} = \frac{k_6[Br^-][Br^{\bullet}]_0}{k_a^{I}}\{1 - e^{-k_a^{I} t}\}\, e^{-\gamma t} \qquad (15)$$

To analyze the data, the absorbance due to $Br_2^{-\bullet}$ can be described by using eq 15 in the Beer−Lambert law (eq 10). Because of the approximation expressed by eq 12, the constant γ is used merely as a fitting parameter and no significance is placed on the values obtained for it.

As can be seen in Figure 2, an intense pulse of scattered laser light contributes to the signals. Because the laser pulse duration (~10 ns) is much shorter than the instrument time constant $\tau_{inst} \approx 0.3-0.5$ μs, the signal from the scattered light decays with a time constant equal to τ_{inst}. During the first 5 μs, the scattered

laser light is strong and must be included in the data analysis. It was found empirically that the scattered laser light is well-approximated by an exponential function. Thus, the observed signal can be described using the Beer−Lambert law plus an exponential term to account for the scattered laser light:

$$I(t) = I_0 \times 10^{-\alpha s[Br_2^{-\bullet}]} + I_{scat}\, e^{-t/\tau_{inst}} \qquad (16)$$

where I_{scat} is the initial intensity of the scattered laser light.

In each series of experiments, the instrument response time constant τ_{inst} was obtained via a least-squares analysis of the scattered light intensity observed using purified water in the cell. In each experiment, the incident intensity I_0 from the pretrigger data was used with eq 16 in a least-squares analysis to obtain the scattered light intensity I_{scat} and rate constant k_a^I. The nonlinear least-squares analysis was carried out using KaleidaGraph (v. 3.5, Synergy Software), which utilizes the Marquardt−Levenberg algorithm.[34,35] A typical nonlinear least-squares fit is shown as the solid line in Figure 2. By plotting values of k_a^I as a function of [Br $^-$], the slope and intercept of the resulting straight line give k_6 and $k_{-6} + (k_8 + k_9)$[DBE], respectively.

Reactions 7−9 were investigated in two types of experiments. On short time scales (= 100 μs), reactions 8 and 9 could be determined using equations 13 and 16, as described above. On long time scales (>100 μs), the reaction mechanism is comprised of reactions 6, −6, 7, 8, and 9, and the pseudo-steady state (SS) approximation is valid for Br$^\bullet$ atoms:

$$[Br^\bullet]_{ss} = k_{-6}[Br_2^{-\bullet}]/(k_6[Br^-] + k_8[DBE]) \qquad (17)$$

By using eq 17, [$Br_2^{-\bullet}$] is described by a second-order differential equation

$$(d[Br_2^{-\bullet}]/dt) = k_b^I[Br_2^{-\bullet}] - k^{II}[Br_2^{-\bullet}]^2 \qquad (18a)$$

where

$$k_b^I = \left(\frac{k_8}{(k_6/k_{-6})\,[Br^-] + (k_8[DBE]/k_{-6})} + k_9\right)[DBE] \qquad (18b)$$

$$k^{II} = (2k_7/\epsilon) \qquad (18c)$$

Equation 18 has the following analytical solution for the mixed first- and second-order kinetics:[36,37]

$$[Br_2^{-\bullet}] = \frac{1}{\epsilon s}\left\{e^{k_b^I t}\left[\frac{1}{A_0} + \frac{k^{II}}{k_b^I s}\right] - \frac{k^{II}}{k_b^I s}\right\}^{-1} \qquad (19)$$

The absorbance due to $Br_2^{-\bullet}$ can be described by using eq 19 in the Beer−Lambert law (eq 10) (scattered laser light does not interfere on this time scale). The experiments were carried out by varying [DBE] from 2.1×10^{-3} M to 1.6×10^{-2} M and [Br$^-$] from 1×10^{-5} M and 5×10^{-3} M. For each DBE concentration, wire screens were used to attenuate the laser energy so that [Br$^\bullet$]$_0$ was $\sim 3 \times 10^{-7}$ M in all experiments.

3.2. Numerical Simulations. To test the accuracy of the approximation described by eq 12, numerical simulations were carried out for a mechanism consisting of reactions 6, −6, 7, 8, and 9. The numerical simulations were carried out using a modified version of CHEMK,[38] which uses the Gear algorithm for numerical integration of stiff ordinary differential equations. Simulations were carried out using a range of [Br$^\bullet$]$_0$ and [Br$^-$] typical of the experiments and the values for k_6 and k_{-6} found in the experiments. A literature value[39] of rate constant $k_7 = 1.9 \times 10^9$ M^{-1} s^{-1} was consistent with our present experiments (see below). The resulting time-dependent [$Br_2^{-\bullet}$] values were used in eq 16 (but omitting the term for scattered laser light) to generate sets of simulated experimental data that were then analyzed in the same manner as the actual experimental data. The analysis of the simulated data generally showed very good agreement with the rate constants obtained from the experiments. At low [Br$^-$], the errors are of the order of a few percent, because reaction 6 is so slow that reaction 7 becomes more important and the approximation in eq 12 is no longer as accurate. The resulting maximum error in the extrapolated intercept of a plot of k_a^I vs [Br$^-$] is ≤10%. This error is included with others in the error analysis described below.

At equilibrium, the Br$^\bullet$ and $Br_2^{-\bullet}$ relative concentrations are controlled by [Br$^-$] according to [$Br_2^{-\bullet}$]/[Br$^\bullet$] = K_6[Br$^-$]. At low [Br$^-$], the [$Br_2^{-\bullet}$]/[Br$^\bullet$] ratio is small and Br$^\bullet$ contributes to the absorption. Because we are using the absorption to determine [$Br_2^{-\bullet}$], it is important to determine the interference from Br$^\bullet$. In a given experiment, the absorbance immediately after the laser pulse is solely due to Br$^\bullet$. As time advances, the absorbance increases, due to consumption of Br$^\bullet$ and concurrent quantitative production of $Br_2^{-\bullet}$, which absorbs much more strongly. When [Br$^-$] is large enough, the maximum absorption is almost entirely due to $Br_2^{-\bullet}$. Eventually, the $Br_2^{-\bullet}$ decays away on a much slower time scale. For a given laser pulse energy, we measured the initial absorbance (due to Br$^\bullet$) in experiments with [Br$^-$] = 0 for comparison with the maximum absorbance (due to $Br_2^{-\bullet}$) measured in experiments with [Br$^-$] = 10^{-5} M. From the ratio of the absorbances, we obtained the ratio of the absorption coefficients: $\alpha_{Br_2^{-\bullet}}/\alpha_{Br^\bullet} \approx 20$ at 365 nm. This result is in very good agreement with an estimate ($\alpha_{Br_2^{-\bullet}}/\alpha_{Br^\bullet} \approx 22$) obtained by extrapolating the data of Kläning and Wolff[40] to 365 nm.

In principle, it is possible to include the absorbance due to Br$^\bullet$ in the least-squares analysis but to do so requires introducing additional fitted parameters. In tests of this approach, we found that the nonlinear least-squares analysis resulted in highly correlated and hence uncertain results because the absorbance due to Br$^\bullet$ is typically of the order of the noise in an individual experiment. Numerical simulations showed that the absorption due to Br$^\bullet$ contributes less than 5% of the absorption after the first 1−2 μs (95% is due to $Br_2^{-\bullet}$) when [Br$^-$] = 10^{-5} M. At lower [Br$^-$], the Br$^\bullet$ contribution drops below 5% of the absorption only after ~5 μs. Therefore, in the results reported here, the data prior to 1 μs were neglected in the least-squares analysis of all experiments with [Br$^-$] = 10^{-5} M and data prior to 5 μs were neglected in the analysis of experiments with [Br$^-$] < 10^{-5} M.

3.3. Determination of k_7 and k_8. Reaction rate constant k_7 can only be determined accurately on longer time scales because it is slow. By using eqs 18c and 19, the rate constant at ~20 °C was found to be $k_7 = (1.9 \pm 0.1) \times 10^9$ M^{-1} s^{-1}, in good agreement with literature values.[39,41] In experiments performed at 54 °C, we obtained $k_7 = (3.3 \pm 0.1) \times 10^9$ M^{-1} s^{-1}, less than twice as large as the result obtained near 20 °C, indicating that k_7 does not depend strongly on temperature. Experiments on the temperature dependence of k_7 are still underway, and the full results will be published later.[42]

Pseudo-first-order rate constant k_b^I is only weakly dependent on [DBE]. A plot of k_b^I vs [Br$^-$] at a fixed [DBE] = 2.1×10^{-3} M shows reasonable agreement with eq 18b if k_9 is neglected. This indicates that the hydrogen abstraction by $Br_2^{-\bullet}$ is less important than reaction 8, which is found to be k_8 =

TABLE 1: Rate Constants and Equilibrium Constants[a]

series	T (°C)	k_6 (10^{10} M^{-1} s^{-1})	$\pm\sigma_6$ (10^{10} M^{-1} s^{-1})	k_{-6} (10^4 s^{-1})	$\pm\sigma_{-6}$ (10^4 s^{-1})	K_6 (10^5 M^{-1})	$\pm\sigma_{eq}$ (10^5 M^{-1})
1	10.5	0.82	0.01	1.47	0.16	5.58	0.48
2	10.5	0.85	0.01	1.44	0.21	5.90	0.67
3	10.5	0.80	0.01	1.53	0.26	5.23	0.71
average	10.5	0.82	0.01	1.47	0.11	5.58	0.34
4	20.0	1.10	0.02	2.55	0.38	4.31	0.54
5	20.0	1.07	0.01	2.75	0.17	3.89	0.20
average	20.0	1.08	0.01	2.73	0.15	3.60	0.19
6[b]	19.5	1.01	0.03	2.56	0.55	3.95	0.71
7[b]	19.5	1.01	0.02	2.34	0.29	4.32	0.43
average	19.5	1.01	0.02	2.38	0.26	4.24	0.37
8	32.0	1.35	0.01	4.48	0.12	3.01	0.07
9	32.0	1.40	0.03	3.78	0.57	3.70	0.48
average	32.0	1.36	0.01	4.45	0.12	3.05	0.07
10	40.0	1.54	0.02	5.35	0.24	2.89	0.11
11	40.0	1.62	0.02	5.65	0.26	2.87	0.12
average	40.0	1.58	0.01	5.47	0.17	2.89	0.08
12	50.0	1.82	0.02	9.66	0.16	1.88	0.03
13	50.0	1.87	0.03	8.58	0.30	2.18	0.07
14	50.0	1.88	0.03	8.06	0.31	2.33	0.09
average	50.0	1.85	0.02	9.20	0.12	2.01	0.03
15[c]	20.0	0.97	0.02	2.06	0.04	4.71	0.75
16[d]	20.0	0.95	0.01	2.54	0.01	3.74	0.15

[a] Relative uncertainties (one standard deviation) from all sources of error in the rate constants and equilibrium constant are ~10% in k_6, ~25% in k_{-6}, and ~30% in K_6. Except as noted, all solutions were pH ≈ 3 and contained dissolved air. [b] Solution purged with helium. [c] pH 1.3. [d] pH 5.3.

$(1.0 \pm 0.3) \times 10^6$ M^{-1} s^{-1} at 17 °C. This value is close to the literature value, 1×10^6 M^{-1} s^{-1}, which was only roughly estimated.[43] However, rate constant k_{-6} is not obtained with precision by the least-squares analysis.

On short time scales, a plot of the pseudo-first-order rate constant k_a^I vs [DBE] gives slope $(k_8 + k_9) = (5 \pm 2) \times 10^5$ M^{-1} s^{-1} at 22 °C, a value roughly consistent with that obtained above and slightly lower than the estimate in the literature.[43] Experiments performed on long time scales at higher temperatures give an activation energy of ~24 ± 6 kJ mol^{-1}. Experiments on k_8 and k_9 are still underway, and the full results will be published later,[42] but it seems appropriate to account for reaction 8 in the data analysis for k_6 and k_{-6}. For that purpose, we will tentatively assume $k_8 = 2 \times 10^{10}\exp(-2890/T)$ M^{-1} s^{-1}. The magnitude of the correction (= k_8[DBE]) is ~10% and even if our ongoing experiments give values for k_8 that differ by as much as 50% from this preliminary result, the associated changes in k_{-6} and K_6 will be much smaller than the estimated uncertainties (see Section 3.6).

3.4. Determination of k_6, k_{-6}, and K_6. Experiments were carried out over a range of conditions, and the results are summarized in Table 1. Measured pseudo-first-order rate constants greater than $\sim 5 \times 10^5$ s^{-1} were rejected, because they may be affected by the instrument response time. Typical results at different temperatures are shown in Figure 3. Each series consisted of at least five experiments containing added bromide ion and at least one blank run with purified water; some series also included blank runs containing just DBE and purified water (no added bromide). In all cases, k_a^I is a linear function of [Br^-] within experimental error, as expected. The slope and intercept were obtained by unweighted linear least-squares. Equal weights were used because the experimental errors are essentially equal within each experiment series. From eq 13d, the slope and intercept correspond to rate constants k_6 and the quantity $k_{-6} + (k_8 + k_9)$[DBE], respectively. As discussed above, k_{-6} was obtained by neglecting k_9 assuming that $k_8 = 2 \times 10^{10}\exp(-2890/T)$ M^{-1} s^{-1}. The equilibrium constant is obtained from the ratio $K_6 = k_6/k_{-6}$. For each experiment series in Table 1, the errors ($\pm\sigma$, one standard deviation) associated with k_6 and k_{-6} are measures of precision only, as obtained from the least-squares analysis; those associated with K_6 were obtained by propagation of errors. The weighted averages of the values for k_6, k_{-6}, and K_6 at each temperature are given in Table 1, where the errors ($\pm\sigma$) indicate precision only. The results are presented as functions of $1/T$ in Figure 5.

Dissolved oxygen is not expected to influence the results,[24,29] and most experiments were carried out using reagent solutions that were exposed to ambient air. The effect of dissolved air was tested by carrying out several series of experiments after purging the solutions with high purity helium gas for 20 min. The results obtained with purged solutions (series 7; see Table

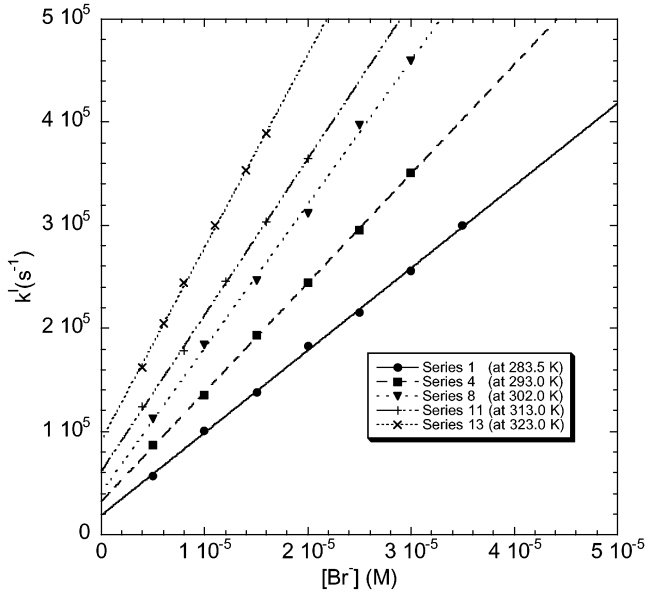

Figure 3. Pseudo-first-order rate constants (k^I) vs [Br^-] at various temperatures (see Table 1).

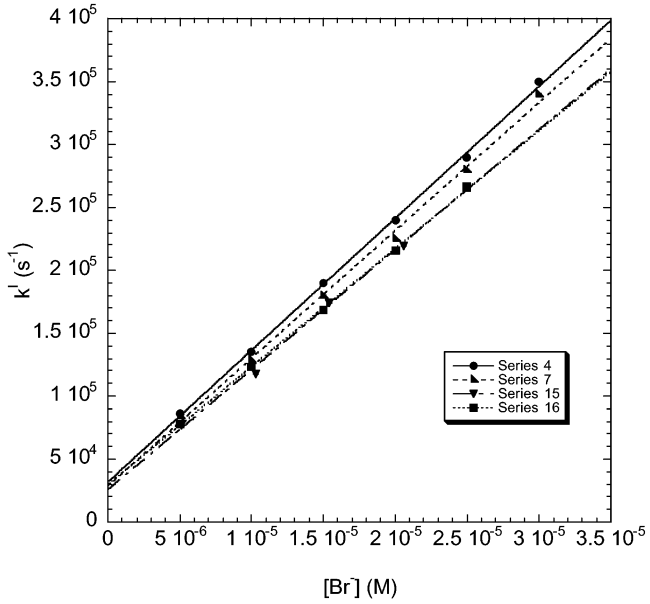

Figure 4. Pseudo-first-order rate constants vs [Br^-] for various conditions (see Table 1).

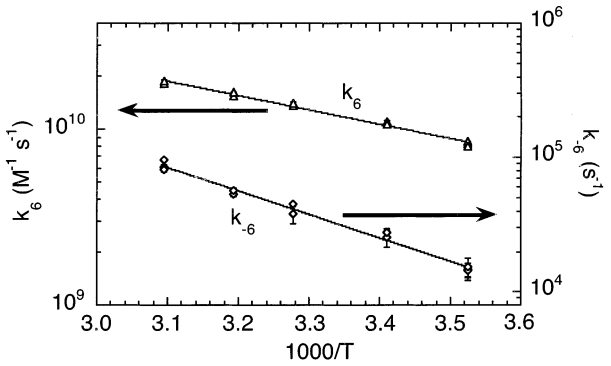

Figure 5. Forward (k_6) and reverse (k_{-6}) rate constants vs $1/T$ (solid lines are nonlinear least-squares fits). Error bars ($\pm\sigma$) indicate precision only. Relative uncertainties (one standard deviation) from all sources of error are ~10% in k_6 and ~25% in k_{-6} (see text for details).

1 and Figure 4) are indistinguishable from those obtained without purging (series 4).

The acidity of the solutions was not expected to influence the results and most experiments were carried out at pH ≈ 3, where the pH was adjusted nominally by adding measured volumes of perchloric acid. However, to test for possible pH effects, experiment series 15 and 16 were conducted at pH 1.3 and pH 5.3, respectively (measured using a pH meter equipped with a glass electrode). The results as represented by Table 1 and Figure 4 are indistinguishable from the experiments carried out at pH ≈ 3.

3.5. Arrhenius Parameters. A nonlinear least-squares analysis was carried out using the average rate constants obtained at each temperature (Table 1). All of the rate constants were assumed to have equal weights. The results are shown as straight lines in Figure 5 and given by eq 20, where the standard deviations and covariances reflect the precision of the experiments. Propagation of errors (including the covariances) shows that the relative error ($\pm\sigma/k$) in k_6 is only a few percent, while that of k_{-6} is less than 10% over the entire temperature range of the experiments. However, there are several potential sources of systematic error, as discussed in the next section.

$$k_6 = (5.11 \pm 0.98) \times 10^{12} \exp(-1812 \pm 60/T)\ \mathrm{M\ s^{-1}},$$
$$\sigma_{AE}{}^2 = 9.78 \times 10^{11}\ \mathrm{M\ s^{-1}\ K} \quad (20a)$$

$$k_{-6} = (2.54 \pm 2.03) \times 10^{10} \exp(-4068 \pm 255/T)\ \mathrm{s^{-1}},$$
$$\sigma_{AE}{}^2 = 2.04 \times 10^{10}\ \mathrm{s^{-1}\ K} \quad (20b)$$

where $\sigma_{AE}{}^2$ is the covariance between the A factor and E_a/R (expressed in units of K), where E_a is the activation energy and R is the gas law constant.

3.6. Potential Systematic Errors. Systematic errors can arise from several sources in the present work. These include the approximations used in deriving eq 13, the limitations due to instrument response time, the effects of temperature differences in the cell, and the effects of impurities.

As described above, numerical tests of the approximations used in deriving eq 15 showed that the maximum error was ~5%. In particular, k_6 was hardly affected at all, while k_{-6} was affected by a maximum of 5%. This maximum 5% error will also affect the equilibrium constant K_6. Thus, we assume that the approximations used in the analysis have no affect on k_6 and affect both k_{-6} and K_6 by 5%.

Instrument response time limitations will affect rate constants that are of the order of the inverse instrument response time ($1/\tau_{inst} \approx 3 \times 10^6\ s^{-1}$) by making the measured rate constants lower than the correct values. Because we only employed rate constants with $k_a{}^I \le 5 \times 10^5\ s^{-1}$, none of the results are affected significantly: the results in Figure 3 show no systematic deviations from straight lines.

In some experiments, the measured temperatures exhibit differences of ~0.5 °C between the entrance and the exit of the cell. At the ends of the temperature range, the differences can sometimes be as large as 1.5 °C. According to the Arrhenius parameters given below, a temperature difference of 1 K causes a variation of 4.5 and 2.2% in k_{-6} and k_6, respectively, and about 4.8% variation in K_6.

The solubility of DBE found in this work is in good agreement with the reported value,[30] as discussed above, and there is a small temperature dependence. Because ambient laboratory temperatures can vary from day to day, the "saturated" solutions may vary in DBE concentration. Taking our measured solubility temperature derivative ($\sim 2.6 \times 10^{-3}\ K^{-1}$) and typical temperature variations that did not exceed 2 °C, we find only ~1% variation of DBE concentration.

Perhaps the largest potential source of systematic errors is the effect of impurities. Because of the fast rate constants and the limitations due to the instrument response time, only low concentrations of Br^- can be used. Because the DBE contains impurities and because it can hydrolyze to produce dissolved bromide ions, precautions were taken to reduce impurities, as discussed above. In experiments using 10% saturated DBE solutions in the absence of added Br^-, an initial absorbance due to $Br^\bullet$ was observed, followed by a slow increase of absorption, possibly due to Br^- impurities in the DBE.

Numerical simulations were used to estimate the concentration of the Br^- impurities. The simulations included only reactions 6, −6, and 7 and used the rate constants found in this work. Because reactions 8 and 9 were neglected, the results correspond to an estimate of the upper limit to the Br^- impurity. The simulations indicate that the Br^- impurity may be as large as $\sim 3 \times 10^{-7}$ M in the room temperature experiments and $\sim 6 \times 10^{-7}$ M at 323 K; this latter concentration is only 12% of the lowest concentration of added Br^- used in the experiments (5×10^{-6} M). The experiments with and without added Br^- are reasonably consistent but show random fluctuations that are larger than the measurement precision. The fluctuations may be due in part to varying amounts of Br^- impurities, especially at higher temperatures where the hydrolysis of DBE is expected to be more rapid. If, on the average, a small concentration of Br^- impurity is present at a given temperature, then $k_a{}^I$ will on the average be increased; this will directly affect k_{-6}, but not k_6, and the equilibrium constant K_6 will be an upper limit to the correct value. According to the numerical simulations, the contribution of Br^- impurities may bring as much as 10% error to the rate constants. However, the experimental results were not sensitive to further washing of the DBE and the rate constants did not show exceptionally large fluctuations. Hence, we estimate that added impurities probably affect k_6 very little and k_{-6} by less than 20%.

Taking into account these potential systematic errors, we conclude that k_6, k_{-6}, and K_6 may be affected by up to ~10, ~25, and ~30% (one standard deviation), respectively. As discussed below, error limits significantly smaller than this are obtained from the nonlinear least-squares analysis for Arrhenius parameters when the covariance between the preexponential factors and the activation energies is included. Thus, we estimate that the relative errors in the results for k_6, k_{-6}, and K_6 are ~10, ~25, and ~30% (one standard deviation) at all temperatures in

TABLE 2: Comparisons of Rate Constants and Equilibrium Constants (Room Temperature)

k_6 (10^{10} M^{-1} s^{-1})	k_{-6} (10^4 s^{-1})	K_6 (10^5 M^{-1})	technique[a]	ref
		2.2	PR	28
~1			PR	46
		0.033	LFP	23
1.1 ± 0.1	70 ± 20	0.16	PR	24
		1.1	PR	26
1.2	3.5		LFP	51
0.9			LFP	45
0.77			PR	52
1.1 ± 0.1			PR	47
1.0 ± 0.5	4.5	2.2	PR	27
		~5.4	PR	29
1.2	1.9	6.3	PR	25
1.2 ± 0.1	3.0 ± 0.8	3.9 ± 1.2	LFP	this work (298 K)

[a] LFP = laser flash photolysis; PR = pulse radiolysis.

the range of the experiments (10.5−50 °C), as expressed in eq 21.

$$k_6 \pm 10\% = 5.1 \times 10^{12} \exp(-1812/T)\ M^{-1}\ s^{-1} \quad (21a)$$

$$k_{-6} \pm 25\% = 2.5 \times 10^{10} \exp(-4068/T)\ s^{-1} \quad (21b)$$

$$K_6 \pm 30\% = 2.0 \times 10^{2} \exp(2256/T)\ M^{-1} \quad (21c)$$

The preexponential factor and temperature dependence of K_6 yield estimates of the entropy and enthalpy of reaction

$$\Delta H_R^\circ = -19 \pm 2\ kJ\ mol^{-1} \quad (22a)$$

$$\Delta S_R^\circ = 44 \pm 6\ J\ mol^{-1}\ K^{-1} \quad (22b)$$

4. Discussion

In the present experiments, the reaction system was kept as simple as possible and consisted of only five reactions: rate constants for two of these were measured quantitatively, and the rest had little effect on the first two. As in all experiments, there are potential sources of error, but even after their possible contributions were considered, the results are known to be reasonably accurate. Our rate constant results are compared with those from previous investigations in Table 2, where it is apparent that our results for k_6 are at the upper end of the range and those for k_{-6} and K_6 are closer to the middle of the range. Although the rate constants and equilibrium constant have been studied previously in several investigations at room temperature,[27,31,44−47] only one previous temperature-dependent measurement has been reported.[29]

Although the temperature-dependent equilibrium constants from the present work overlap with those of Kosaníc at lower temperatures, the slopes of the van't Hoff plots are significantly different: the value for ΔH_R° found in the present experiments is about 10 kJ mol^{-1} smaller than that reported by Kosaníc.[29] The reason for this difference is not apparent. To determine the equilibrium constant, Kosaníc employed pulse radiolysis of oxygen-saturated solutions containing bromide and oxalic acid. In contrast to the simplicity of the present reaction system, Kosaníc's mechanism included a half-dozen or more reactions. Kosaníc carried out the analysis in two ways. (i) By assuming no losses of free radicals, it is possible to use the total radical yield from a given dose rate and the measured concentration of $Br_2^{-\bullet}$ (with $\alpha = 9600\ M^{-1}\ cm^{-1}$, base 10) to obtain K_6. (ii) By considering the decay of $Br_2^{-\bullet}$ via reaction 7 in and via the reaction of $Br^\bullet$ with oxalic acid, it is possible to obtain K_6. The latter method required measurement of the rate constant for $Br^\bullet$ + oxalic acid, as well as accurate radical yield actinometry and an accurate literature value for rate constant k_7. Possible sources for the discrepancy with the present work include the temperature dependence of the free radical actinometry, the rate constant for the $Br^\bullet$ + oxalic acid reaction, and possible interference from other reactions. Kosaníc's reported results are internally consistent and of high precision, but he did not discuss potential sources of uncertainty.

The activation energies for reactions 6 and −6 may arise from different sources. Reaction −6 is a dissociation reaction and hence may be endothermic. On the other hand, the rate constant for reaction 6 is near the diffusion limit; hence, the activation energy may be due to diffusion control.

The diffusion-controlled rate constant may be written[48]

$$k_D = \frac{4\pi N_A (D_A + D_B)(r_A + r_B)}{1000} \quad (23)$$

where D_A and D_B are the diffusion coefficients for reactants A and B and r_A and r_B are the respective radii; N_A is Avogadro's number. The Stokes−Einstein relationship (eq 24) relates the diffusion coefficient to the viscosity η. By assuming that η corresponds to that of water and assuming that $Br^\bullet$ and Br^- have approximately the same radii and the same diffusion coefficients in water, we obtain the relation between diffusion-controlled rate constant k_D and viscosity shown by eq 25.

$$D = (kT/6\pi r\eta) \quad (24)$$

$$k_D = (8RT/3000\eta) \quad (25)$$

The temperature-dependent viscosity (expressed in units of centipoise) of water can be expressed as follows:[49]

$$\log \eta(T) = -10.2158 + 1792.5/T + 0.01773T - 1.2631 \times 10^{-5} T^2 \quad (26)$$

The activation energy of k_D is based on the Arrhenius expression

$$E_D = -R\{d(\ln k)/d(1/T)\} = -R[T^2\{d(\ln \eta(T))/dT\} - T] \quad (27)$$

At 298 K, the activation energy is estimated to be $E_D \approx 10$ kJ mol^{-1}, a bit lower than the activation energy found for reaction 6 but within the typical range of activation energies for diffusion-controlled reactions (8−24 kJ mol^{-1}). Considering the simplifying approximations used above to calculate E_D, the agreement is satisfactory and supports the conclusion that reaction 6 is diffusion-controlled.

The reduction potential corresponding to reaction 6 is related to the equilibrium constant and to the standard reduction potentials for two couples[50]

$$\Delta E_6^\circ/V = 0.0591 \log(K_6) \quad (28a)$$

$$\Delta E_6^\circ = E^\circ(Br^\bullet/Br^-) - E^\circ(Br_2^{-\bullet}/2Br^-) \quad (28b)$$

From eq 21c, we have $K_6 = (3.9 \pm 1.2) \times 10^5\ M^{-1}$ at 298 K, giving $\Delta E_6^\circ = 0.33 \pm 0.01$ V, according to eq 28a. This result can be compared with the value obtained using eq 28b. The recently reported[25] standard reduction potentials vs NHE for

the couples in eq 28b are $E°$ ($Br^{\bullet}/Br^{-}$) = 1.94 V and $E°$ ($Br_2^{-\bullet}/2Br^{-}$) = 1.66 V. The result is $\Delta E_6° = 0.32$ V, in very good agreement with the value obtained from the present value of K_6.

Acknowledgment. Thanks go to the Atmospheric Chemistry Division of NSF for support of this work.

References and Notes

(1) Barrie, L. A.; Bottenheim, J. W.; Schnell, R. C.; Crutzen, P. J.; Rasmussen, R. A. *Nature* **1988**, *334*, 138.
(2) Bottenheim, J. W.; Barrie, L. A.; Atlas, E.; Heidt, L. E.; Niki, H.; Rasmussen, R. A.; Shepson, P. B. *J. Geophys. Res.* **1990**, *95*, 18555.
(3) McConnell, J. C.; Henderson, G. S.; Barrie, L.; Bottenheim, J.; Niki, H.; Langford, C. H.; Templeton, E. M. J. *Nature* **1992**, *355*, 150.
(4) Mozurkewich, M. *J. Geophys. Res.* **1995**, *100*, 14199.
(5) Fan, S.-M.; Jacob, D. J. *Nature* **1992**, *359*, 522.
(6) Sander, R.; Crutzen, P. J. *J. Geophys. Res.* **1996**, *101*, 9121.
(7) Oum, K. W.; Lakin, M. J.; DeHaan, D. O.; Brauers, T.; Finlayson-Pitts, B. j. *Science* **1998**, *279*, 74.
(8) Oum, K. W.; Lakin, M. J.; Finlayson-Pitts, B. J. *Geophys. Res. Lett.* **1998**, *25*, 3923.
(9) Finlayson-Pitts, B. J.; Hemminger, J. C. *J. Phys. Chem. A* **2000**, *104*, 11463.
(10) Foster, K. L.; Plastridge, R. A.; Bottenheim, J. W.; Shepson, P. B.; Finlayson-Pitts, B. J.; Spicer, C. W. *Science* **2001**, *291*, 471.
(11) Jayson, G. G.; Parsons, B. J.; Swallow, A. J. *J. Chem. Soc., Faraday Trans. 1* **1973**, *69*, 1597.
(12) Huie, R. E. Free radical chemistry of the atmospheric aqueous phase. In *Progress and Problems in Atmospheric Chemistry*, 1st ed.; Barker, J. R., Ed.; World Scientific: Singapore, 1995; p 374.
(13) Yu, X.-Y.; Bao, Z.-C.; Barker, J. R. *J. Phys. Chem. A* **2002**, manuscript in preparation.
(14) Yu, X.-Y. Kinetics of Free Radical Reactions Generated by Laser Flash Photolysis of $OH+Cl^-$ and $SO_4^-+Cl^-$ in the Aqueous Phase—Chemical Mechanism, Kinetics Data and Their Implications. Ph.D. Thesis, The University of Michigan, 2001.
(15) Prutz, W. A.; Butler, J.; Land, E. J. *Int. J. Radiat. Biol. Relat. Stud. Phys. Chem. Med.* **1985**, *47*, 149.
(16) Adams, G. E.; Aldrich, J. E.; Bisby, R. H.; Cundall, R. B.; Redpath, J. L.; Willson, R. L. *Radiat. Res.* **1972**, *49*, 278.
(17) Adams, G. E.; Bisby, R. H.; Cundall, R. B.; Redpath, J. L.; Willson, R. L. *Radiat. Res.* **1972**, *49*, 290.
(18) Finlayson-Pitts, B. J.; Pitts, J. N., Jr. *Chemistry of the Upper and Lower Atmosphere*; Academic Press: San Diego, 2000.
(19) Zafiriou, O. C.; True, M. B.; Hayon, E. Consequences of OH radical reaction in seawater: Formation and decay of Br_2^- ion radical. In *Photochemistry of Environmental Aquatic Systems*; American Chemical Society: Washington, DC, 1987; p 89.
(20) Wu, D.; Wong, D.; Bartolo, B. D. *J. Photochem.* **1980**, *14*, 303.
(21) Adams, D. J.; Barlow, S.; Buxton, G. V.; Malone, T. N.; Salmom, G. A. *J. Chem. Soc., Faraday Trans. 1* **1995**, *91*, 3303.
(22) Buxton, G. V.; Bydder, M.; Salmon, G. A. *J. Chem. Soc., Faraday Trans. 1* **1998**, *94*, 653.
(23) Wong, D.; Bartolo, B. D. *J. Photochem.* **1975**, *4*, 249.
(24) Treinin, A.; Hayon, E. *J. Am. Chem. Soc.* **1975**, *97*, 1716.
(25) Merényi, G.; Lind, J. S. *J. Am. Chem. Soc.* **1994**, *116*, 7872.
(26) Mamou, A.; Rabani, J.; Behar, D. *J. Phys. Chem.* **1977**, *81*, 1447.
(27) Lind, J.; Shen, X.; Eriksen, T. E.; Merenyi, G.; Eberson, L. *J. Am. Chem. Soc.* **1991**, *113*, 4629.
(28) Matheson, M. S.; Mulac, W. A.; Weeks, J. L.; Rabani, J. *J. Phys. Chem.* **1966**, *70*, 2092.
(29) Kosaníc, M. M. *J. Serb. Chem. Soc.* **1993**, *58*, 55.
(30) McConnel, J. B.; et al. *Investigation of Ethylene Dibromide (EDB) in Groundwater in Seminole County, Georgia*; U.S. Geological Survey, 1984.
(31) Weldon, D.; Barra, M.; Sinta, R.; Scaiano, J. C. *J. Org. Chem.* **1995**, *60*, 3921.
(32) Scaiano, J. C.; Barra, M.; Calabrese, G.; Sinta, R. *J. Chem. Soc., Chem. Commun.* **1992**, 1418.
(33) Cercek, B.; Ebert, M.; Gilbert, C. B.; Swallow, A. J. *Pulse radiolysis of aerated aqueous potassium bromide solutions*; Presented at the International Symposium on Pulse Radiolysis, Manchester, 1965.
(34) Marquardt, D. W. *J. Soc. Ind. Appl. Math.* **1963**, *11*, 431.
(35) Bevington, P. R. *Data Reduction and Error Analysis for the Physical Sciences*; McGraw-Hill: New York, 1969.
(36) McElroy, W. J. *J. Phys. Chem.* **1990**, *94*, 2435.
(37) Bao, Z.-C.; Barker, J. R. *J. Phys. Chem.* **1996**, *100*, 9780.
(38) Whitten, G. Z.; Hogo, H. *CHEMK*; Science Applications Inc.: 1980.
(39) Ross, A. B.; Bielski, B. H. J.; Buxton, G. V.; Cabelli, D. E.; Greenstock, C. L.; Helman, W. P.; Huie, R. E.; Neta, P. NDRL/NIST Solution Kinetics Database, NIST Standard Reference Database 40, 1.0 ed.; National Institute of Science and Technology: Gaithersburg, MD, 1992.
(40) Kläning, U. K.; Wolff, T. *Ber. Bunsen-Ges. Phys. Chem.* **1985**, *89*, 243.
(41) Ferraudi, G. *J. Phys. Chem.* **1993**, *97*, 2793.
(42) Pimentel, A. S.; Barker, J. R. Unpublished results.
(43) Lal, M. *Radiat. Phys. Chem.* **1988**, *32*, 741.
(44) Scaiano, J. C.; Barra, M.; Krzywinski, M.; Sinta, R.; Calabrese, G. *J. Am. Chem. Soc.* **1993**, *115*, 8340.
(45) Nagarajan, V.; Fessenden, R. W. *J. Phys. Chem.* **1985**, *89*, 2330.
(46) Zehavi, D.; Rabani, J. *J. Phys. Chem.* **1972**, *76*, 312.
(47) Neta, P.; Huie, R. E.; Ross, A. B. *J. Phys. Chem. Ref. Data* **1988**, *17*, 1027.
(48) Steinfeld, J. I.; Francisco, J. S.; Hase, W. L. *Chemical Kinetics and Dynamics*, 2 ed.; Prentice-Hall: New York, 1998.
(49) Yaws, C. L. *Chemical Properties Handbook: Physical, Thermodynamic, Environmental, Transport, Safety, and Health Related Properties for Organic and Inorganic Chemicals*; McGraw-Hill: New York, 1999.
(50) Wardman, P. *J. Phys. Chem. Ref. Data* **1989**, *18*, 1637.
(51) Lilie, J.; Koskikallio, J. *Acta Chem. Scand., Ser.* **1984**, *38*, 41.
(52) Lal, M.; Moenig, J.; Asmus, K.-D. *Free Radical Res. Commun.* **1986**, *1*, 235.